

The Stone-Wales transformation: from fullerenes to graphite, from radiation damage to heat capacity

M.I. Heggie^{1,2†*}, G.L. Haffenden¹, C.D. Latham², T. Trevethan²

¹Department of Chemistry, University of Sussex, Falmer, Brighton BN1 9QJ, United Kingdom

²Department of Chemistry, University of Surrey, Guildford, GU2 7XH, United Kingdom

Keywords: fullerenes, graphite, Local Density Approximation, Dienes defect, Stone-Wales, heat capacity

Summary

The Stone-Wales (SW) transformation, or carbon bond rotation, has been fundamental to understanding fullerene growth and stability, and *ab initio* calculations show it to be a high energy process. The nature and topology of the fullerene energy landscape shows how the I_h -C₆₀ must be the final product, if SW transformations are fast enough, and various mechanisms for their catalysis have been proposed. We review SW transformations in fullerenes and then discuss the analogous transformation in graphite, where they form the Dienes defect, originally posited to be a transition state in the direct exchange of a bonded atom pair. On the basis of Density Functional Theory (DFT) calculations in the Local Density Approximation (LDA) we propose that non-equilibrium concentrations of the Dienes defect arising from displacing radiation are rapidly healed by point defects and that equilibrium concentrations of Dienes defects are responsible for the divergent ultra-high temperature heat capacity of graphite.

Introduction

Within a year of fullerenes being discovered [1] was the famous theory paper that discussed how C₆₀ isomers could be interconverted through rotations of bonded atom pairs about the centre of their bond [2] in what has become known as the Stone-Wales (SW) transformation. The paper underlined the problem – the process is forbidden by the Woodward-Hoffman rules [3] for pericyclic reactions if treated on a par with standard organic reaction chemistry, and would be difficult even if allowance is made for the extreme conditions of fullerene synthesis and condensation. This was an obstacle for understanding the experimental observation of the I_h isomer and none other, as proven by the first C₆₀ ¹³C n.m.r. [4] which comprised a single line arising from a single chemical environment shared by all atoms. The fact that the I_h isomer has global thermodynamic stability for C₆₀ was understood in terms of the Isolated Pentagon Rule (IPR), although a strong indication was given in ref 2 that many other isomers are energetically similar to the I_h one and should be observed.

The isomers of C₆₀ were enumerated [5] and it was apparent that the transformation from an arbitrary isomer to the I_h isomer, must proceed through the C_{2v} isomer, so most calculations focussed on this step. The *ab initio* calculations gave two different saddle points: symmetrical and asymmetrical involving sp^3 carbon [6], but both still with very high activation barriers (respectively, 8.4 and 6.9 eV, taking the highest level of theory at the time: 4s2p1d/BLYP and the largest C₆₀ fragment). The asymmetrical transition state was later dismissed as an artefact of lower levels of theory in a comprehensive review and revision [7], which concluded the activation barrier was 6.9 eV - 7.3 eV through the symmetrical state.

*Author for correspondence (malcolm.heggie@gmail.com).

†Present address: BlackDogBytes, Brin Villa, Black Dog, Devon EX17 4QU, UK

Early work [8,9] by two of us (MIH, CDL) with others based on Density Functional Theory (DFT) in the Local Density Approximation (LDA) within the cluster AIMPRO code [10] showed that trace hydrogen could in principle be responsible for lowering the barrier and facilitate removal of IPR-violating isomers. The reason is that the ground state of $C_{60}H$ is radical [11], pushing up the chemical potential of the molecule, while the transition state is relatively stabilised by a stronger C-H bond than in the ground state. There is also a binding between the H atom and more defective regions of C_{60} isomers, such as neighbouring pentagons, which attracts it to these regions prior to catalysing the transformation.

This idea of a species which makes the ground state less stable and the transition state more stable led to studies of the structure and effects of the carbon adatom [8,12,13]. Using DFT and LDA these confirmed that the $C_{2v} - I_h$ transition of C_{60} is catalysed by an adatom, lowering the barrier from 4.7 to 2.9 eV [12] and that the adatom is attracted to regions which violated the IPR. The carbon growth path through various IPR-violating carbon cages, which resulted ultimately in I_h-C_{60} , could thus be regarded as *auto-catalytic* [12]. Later inspection of another path found an even greater catalytic effect, lowering the barrier to 1.1 eV [13] and importantly carried forward the effect into graphene, which we will return to later.

While our group and others focussed on the catalysis, Wales and co-workers developed an elegant theory of the connectivity of energy valleys, which revealed why I_h-C_{60} is the sole C_{60} product [14]. As an aside, we remark that the same theory, and the relative ease of the SW transformation when auto-catalysed, has been invoked to explain why the hypothetical material pentagraphene is not likely to be stable [15].

Taken with the work on energy landscapes [14], there seems now to be little problem in reconciling the high barrier to the original Stone-Wales transformation with the lack of appearance of non- I_h - isomers. This has been shown very strongly by the most recent work in the area by Prof. Sir Harry Kroto and his collaborators [16], combining DFT and mass spectroscopy measurements. This has shown that fullerenes grow from atomic and clustered carbon, primarily C and C_2 , through 'a closed network growth (CNG) mechanism' demonstrably for C_{60} , C_{70} , C_{76} , C_{78} , C_{84} and some endohedral metallofullerenes. The atomic carbon catalyses bond rearrangements after inclusion in the fullerene shell and the Endo-Kroto mechanism [17], whereby addition of C_2 units across opposing sides of a hexagon, inherently moves pentagons around concomitant with its inclusion. This work identifies the importance of I_h-C_{60} as being the 'bottleneck' in the growth of larger fullerenes, which nevertheless could grow without upper limit. Their approach used a hydrogen atmosphere as a mechanistic probe and showed that fullerene growth could still occur, thus ruling out any mechanism which did not proceed through closed cages. In addition, it showed that adatom SW catalysis could still proceed in the case of a partially hydrogenated adatom (CH), which is distinct from the early calculations of catalysis of SW transformation by H [8].

Also in recent times there have been several works confirming, theoretically, that the SW transformation in fullerenes is catalysed by hydrogen [18] and by adatoms [19].

Now we return to graphene. Almost all early defect calculations claiming to represent graphite were in fact based on graphene, and this goes for nearly all calculations of the vacancy [20-23] and the analogue of the Stone-Wales transformation in graphite [9,13,24]. In the case of finite graphene segments, these generally had hydrogenated edges, and were thus polycyclic aromatic hydrocarbons (PAH).

Initial theory work by Dienes in 1952 on diffusion in graphite considered vacancy diffusion and diffusion by direct exchange of neighbouring atoms [25]. Nowadays hardly any of this work is regarded as quantitative, given the limited computer resources available and the empirical nature of the approximations used. In the Dienes' article, the saddle point (transition state) of direct exchange has the same bonding topology (four carbon cycles, alternately pentagon, heptagon, pentagon, heptagon) as what has become known as the Stone-Wales defect in graphene. Since the first and landmark DFT study of diffusion [24] at the end of the decade that saw the dawn of reliable DFT/pseudopotential calculations, it was apparent this was a metastable state and not a saddle point. Nevertheless, there has recently been a rationalisation of nomenclature proposed [26] which recommends this structure be known as a Dienes defect, which we follow here, while retaining the SW nomenclature for the transformation process.

There is now good experimental evidence for the existence of Dienes or SW defects in graphene from aberration corrected electron microscopy [27,28] and theory confirms that they have properties and activation problems similar to fullerenes [13,29]. Note this includes theory up to the Quantum Monte Carlo level [29]. Furthermore, theory also confirms the same catalytic effect in graphene of adatoms [13,30] and of hydrogen [31-33]. One important difference in graphene compared with fullerenes is the buckling of the carbon network it causes [30] – this is something that was missed in ref. 13, which employed a flat PAH as its model of graphene.

It is striking how the understanding of graphene in the electron microscope has evolved from simple evidence of existence, to the beginnings of quantitative understanding of defect motion and lifetimes [34]. So far, it appears that the catalytic mechanisms of Dienes defect destruction in the electron microscope are not sufficient to explain their unexpectedly low lifetime and furthermore it is enigmatic that their creation at accelerating voltages below the displacement threshold (60 keV) appears little different from that at the threshold (80 keV). For both of these, electronic excitation mechanisms have been suggested [34].

There is a great deal of interest in the radiation damage of graphite, because of its application as a moderator in gas-cooled reactors, particularly the Advanced Gas-cooled Reactors, which are operational in the United Kingdom [35]. Neutron moderation proceeds by absorption of kinetic energy in atomic displacement followed by diffusion of vacancies and interstitials [36], but creation of the Dienes defect can also arise, as has been clearly shown in molecular dynamic simulations [37]. Therefore the question arises as to what the mechanism is for Dienes defect annihilation, given that on its own it is metastable with a large activation barrier against elimination as discussed earlier.

Clearly the catalytic effect of the carbon adatom can substantially lower the barrier for the removal of a Dienes defect in fullerene and graphitic systems. Therefore the stability of a population of Dienes defects will depend on both the concentration and mobility of this intrinsic defect. According to a number of *ab initio* studies, in suspended single layer graphene, an adatom (interstitial) can migrate through the structure with relatively low barriers (0.3 – 0.5 eV [38-40]). However, in the case of the three-dimensional graphite structure the lower energy 'spiro' configuration of the self-interstitial in-between adjacent graphene layers [9,41] significantly decreases the interstitial mobility: the activation energy to leave this state is calculated to be in the range 1.2 – 2 eV [42,43].

It may be case that in the graphite structure the lattice vacancy is more mobile than the interstitial, contrary to historical inferences [44]: both DFT calculations and experimental atomic resolution imaging determine the activation energy for vacancy migration to be in the range 1.0 – 1.2 eV [27,28,45,46] as opposed to the historical inferred value 3.1 eV [44]. Recent calculations have also revealed that the activation energy for mono-vacancy migration is extremely sensitive to the in-layer strain, with the barrier being halved or doubled with uniaxial strains of just 1-2% [47] and it was shown this has a profound effect on vacancy aggregation [48].

In light of the questions concerning the lifetime of Dienes defects under irradiation, we performed calculations to investigate the interaction of diffusing lattice vacancies with Dienes defects. These calculations demonstrate that the strain field created by the Dienes defect has a substantial effect on the mobility of a mono-vacancy in its vicinity, and that a mobile vacancy is attracted towards the areas of compressive strain that surround the Dienes defect. After a vacancy has interacted with a Dienes defect and formed a Dienes-vacancy complex, the barrier for the removal of the Dienes defect via a bond rotation is lowered to 1.2 eV, leaving only the isolated vacancy which can then migrate. In this way, a single diffusing vacancy can 'heal' an unlimited number of Dienes defects.

Finally we shall consider the role of the SW transformation in thermal energy storage: graphite has a very high heat capacity, which was first modelled in DFT in 2005 [49]. It is the basis of commercial heat storage systems operating up to 1000 C and remarkably, above 2000 C graphite's heat capacity has been reported to grow strongly [50-52]. In the third reference, the measurement is ultrafast, so the divergence temperature is much enhanced (around 3200 C). Speculations to date are that this is due to the reversible formation of lattice vacancies [52,53], but it has been suggested [53] this is not compatible with the direct *Phil. Trans. R. Soc. A.*

measurement of vacancy concentrations by etching which gives below 10^{-10} per atomic site [54]. In addition, unless surfaces are involved, increasing the vacancy concentration must be achieved by thermal generation of Frenkel pairs, which have an activation energy greater than the Frenkel pair energy of 14 eV [44,45]. For this reason we do not proceed with the vacancy here.

Here we provide an alternative thermal energy storage mechanism, which is the reversible formation of Dienes defects. The barrier to their formation, which is 9.7 eV [45], is more accessible than that for Frenkel defects and there are reports that heating single-walled carbon nanotubes to 2000 C creates a measureable concentration of these defects [55], as well as indirect evidence, from reduced interlayer separation in multi-walled nanotubes, that they are being created where the temperature exceeds 2800 K [56].

These heat capacity effects involve the Dienes defect in thermal equilibrium, where, as the lowest energy structural defect in graphite, they should be expected to dominate in relative isolation with little or no interaction with the higher energy and much rarer Frenkel defects. Contrarily, in radiation damage the creation of Dienes defects is rapid and they are very far from thermal equilibrium concentrations. Where the radiation is above the displacement threshold, as in a nuclear reactor, a strong flux of Frenkel pairs can be expected, so the interaction of Dienes defects with vacancies and interstitials is important. Thus, after describing the computational models we use, we present results and discussion separately for the two cases: Dienes defect out of thermal equilibrium and Dienes defect in thermal equilibrium. We finish with concluding remarks.

Methods

The DFT-LDA studies reported here use AIMPRO supercell code [57-59], which expands the charge density in plane waves (up to an energy cut-off, E_{cut}). The LDA exchange correlation energy functional was parameterised by Perdew and Wang [60]. Gaussian basis functions centred at atom sites are used to construct the Kohn-Sham wave function. Each radial Gaussian is multiplied by polynomials $x^\alpha y^\beta z^\gamma$, where $\alpha + \beta + \gamma \leq n$; so $n = 0$ gives one function, $n = 1$ gives four and $n = 2$ gives ten. By analogy with atomic angular momentum labels, these are represented by symbols, s, p and d, respectively. Typically four or five exponents are used with different angular variations, and here pdpp is used, unless otherwise specified. Norm-conserving pseudo potentials are based on the Hartwigsen-Goedecker-Hutter scheme [61] and a Monkhorst-Pack (MP) [62] k -point grid is used. Oscillations of charge density in partially degenerate orbitals during the self-consistency cycle are damped using a Fermi occupation function of $k_B T = 0.04$ eV typically, where k_B is the Boltzmann constant and T is absolute temperature. Minimum energy paths between states are determined using the climbing image nudged elastic band method (NEB) [63]. All cells were hexagonal AB-stacked graphite.

Vibrational modes are calculated for the fully optimised structures from the energetic double derivatives, with respect to displacement of each of the atoms. Each atom, a , is displaced a distance, ε (usually 0.02 a.u.) along each axis l , then the charge density is recalculated giving the forces, $f_{mb}^\pm(l, a)$ on each atom, b , in each direction, m . The dynamical matrix in this quasi-harmonic approximation is given by

$$D_{la,mb} = \frac{1}{m_C} \frac{f_{mb}^+(l,a) - f_{mb}^-(l,a)}{2\varepsilon} \quad , \quad (1)$$

where m_C is the atomic mass of carbon, and this matrix yields the square of the vibrational frequencies, ω_j , after diagonalization.

The total lattice heat capacity at constant volume, C_V , at temperature, T , from all the modes is given by the sum

$$C_V = k_B \sum_j \frac{\theta_j^2}{\sinh^2 \theta_j} \quad , \quad (2)$$

where $\theta_j = \frac{\hbar \omega_j}{2k_B T}$, [64]. Since the cell is 18 times the primitive cell, only Gamma point sampling of the phonon Brillouin zone is used.

The total vibrational entropy of a supercell is given by the expression

$$S_{\text{total}} = -k_{\text{B}} \sum_j \left[\ln(1 - e^{-2\theta_j}) - \frac{2\theta_j}{e^{2\theta_j} - 1} \right] . \quad (3)$$

The entropy due to formation of a defect d in a supercell containing n atoms with total entropy S_{total} is then $S_{\text{f}} = S_{\text{total}} - nS_{\text{C}}$, where S_{C} is the entropy per atom for graphite, calculated using a defect-free supercell of comparable size to the one containing d .

The heat capacity contribution from reversible formation of defects of formation energy E_{f} and entropy S_{f} is obtained from [65,66]:

$$C_V = \frac{E_{\text{f}}^2}{k_{\text{B}}T^2} N_0 \exp\left(-\frac{E_{\text{f}}}{k_{\text{B}}T}\right) \exp\left(\frac{S_{\text{f}}}{k_{\text{B}}}\right) , \quad (4)$$

where N_0 is the number of defect sites per mole, which for the Dienes defect is the number of bond centres, *i.e.* 1.5 times Avogadro's number.

For the heat capacity of graphite, 72-atom cells are used with $E_{\text{cut}} = 200$ Ha. These have been checked with 288-atom $6 \times 3 \times 2$ orthorhombic supercell, $E_{\text{cut}} = 248.8$ Ha, an MP mesh of $6 \times 6 \times 3$ k -points and $k_{\text{B}}T = 0.001$ eV using the formalism set out in ref. 59 and similarly for point defects in graphite.

A hexagonal 256-atom (8x8) graphite cell is used for the Dienes defect with full geometry optimisation. The vibrational frequencies are obtained for 80 atoms, in the defect and up to third neighbours of the defect, using only the point (0.5, 0.5, 0.25) in relative coordinates of the electronic Brillouin zone, pppp basis and $E_{\text{cut}} = 175$ Ha.

The stability of Dienes defects in graphene in the presence of point defects is studied in cells of 12×6 times the 4 atom orthorhombic unit cell (288 atoms) with a vacuum gap of 1.3 nm between periodic images in the direction perpendicular to the plane. The MP mesh was $4 \times 4 \times 1$. Energy minima were determined when the maximum force falls below 0.1 eV nm⁻¹ and the NEB chains consisted of 9 images. Activation energies for migration are determined by the height of the saddle-point relative to the energy minimum.

Dienes defect out of thermal equilibrium

Results

The 2D-optimised structure of the Dienes defect in a planar graphene supercell is shown in Fig. 1, coloured according to the in-layer strain. For the purposes of illustration, the out-of-plane displacements were excluded, enhancing the inlayer strain and making it closer to the case of graphite where neighbouring layers inhibit out of plane displacements. Here, it can be seen that the darker areas emanating from the two five-membered rings either side of the defect are under compressive strain, while the lighter coloured areas emanating from the seven-membered rings above and below the defect are under tensile strain. As shown in [47, 48], the activation energy for vacancy migration is very sensitive to the strain. Its dependence on the strain tensor is complex, but it suffices to note here that mobile mono-vacancies will be more mobile in, and hence preferentially accumulate in, areas of compressive strain. In this case it is then expected that when a mobile mono-vacancy diffuses to the vicinity of the Dienes defect it will be rapidly channelled to the five-membered rings. To demonstrate this, we performed a series of DFT calculations for the migration of a mono-vacancy towards the five-membered ring of a Dienes defect, as shown in Fig. 2, where the minimum energy path and barriers between each state were determined with the NEB method and full geometry optimisation was performed to include out-of-plane distortions.

As the vacancy moves from configuration 1 to configuration 5 (where it removes one of the atoms forming the five-fold ring), the energy monotonically decreases and each barrier to be crossed is less than 0.8 eV

(substantially less than in the perfect lattice). The energies of the potential minima and the barriers are depicted in Fig. 3.

When the vacancy has reached configuration 5, the Dienes defect can be healed via a bond rotation (of the atom pair highlighted). This transition is shown in Fig. 4, and is calculated to have a barrier of 1.2 eV, substantially lower than the 5 eV barrier to remove the isolated defect.

The Nudged Elastic Band reaction paths for the catalysed and uncatalysed paths are shown in Fig. 5, showing directly the strong catalytic effect. In these energy profiles, the formation energy of the vacancy is not included, since overall it is unchanged in the reaction. Before elimination of the Dienes defect, the Dienes defect:vacancy complex (fig. 5, left) is strongly bound, by approximately 3 eV.

Discussion

Given a non-equilibrium concentration of Dienes defects at room temperature or even reactor temperatures, how quickly should it fall back to its normally negligible equilibrium concentration? In the case of the electron beams below the displacement threshold the annihilation barrier should be in the region of 7 eV [13]. This would make the destruction rate negligible and the concentration stable, but the observation is that this is not the case for graphene, and an unspecified electronic mechanism has been invoked [34]. Above the displacement threshold, it is already known that the adatom on graphene will catalyse removal: it is a highly mobile species even at room temperature and is attracted to, binds with, and annihilates the Dienes defect [13, 30].

The vacancy in graphene is also mobile, but not at room temperature except in regions of high compressive strain [48], so it is not expected to make an important contribution to the annihilation of the Dienes defect. Nevertheless, in the case of graphite, the interstitial atom is relatively immobile compared with the vacancy and here vacancy catalysed destruction should be important.

The calculations presented are based on graphene: large area cells are needed because of the Dienes defect strain field and a full calculation for graphite of say a four layer cell would require more than a thousand atoms. The weak interlayer interactions are not expected to affect the results strongly, and the reduced out-of-plane distortions in graphite will only serve to enhance in-layer strains (to approach those of Fig. 1) and hence increase the speed of vacancy-Dienes defect complexing and annihilation.

What is clear from the strain map (Fig. 1) and the strain sensitivity of vacancy migration is that vacancies in the vicinity of the Dienes defect should be expected to drift toward the defect along the axis of the two rotating atoms (*i.e.* the horizontal direction of Fig. 1) and then catalyse its destruction. Fig. 2 shows this, where the axis is parallel to the bond between the two red atoms and no longer horizontal. The vacancy swings between alpha and beta sites as it approaches the Dienes defect, culminating at a pentagon site (configuration 5, Fig. 3). The energy landscape is such that the highest barrier traversed is approximately 0.8 eV (from configuration 2 to 3) giving mobility around room temperature. Then it takes an activation of 1.2 eV to annihilate the Dienes defect. The last, rate limiting step should be occurring at a rate of 1 s^{-1} around 160 C. In regions where there is an overall compressive strain field, these energies are expected to reduce strongly.

These data for graphene, should not be dissimilar to those in graphite, and they suggest that Dienes defects should not survive during radiation damage of graphite at typical reactor temperatures, which are in the region of 400 C. This is contrary to the expectation if destruction were not catalysed by point defects.

Dienes defect in thermal equilibrium

Results

Heat capacity calculations relate to isolated Dienes defects in thermal equilibrium. The original calculations [66] of heat capacity based on a 72 atom cell with numerical differentiation as in equation (1) for the dynamical matrix and then diagonalization to produce vibrational frequencies at the Gamma point of the Brillouin zone, gave the saturating curve of Figure 6 for the lattice heat capacity from equation (2). The agreement with measurement below 2000 K is clearly excellent and the 288 atom cell calculations gave results which fall within the line width of the curve of this plot.

The AIMPRO DFT formation energy for the Dienes defect was found to be 5.1 eV and its entropy rises to $7.6 k_B$ at 3500 K. Employing equation (4) gave the additional contribution from reversible formation of Dienes defects, which produced the 'total' heat capacity of Fig. 6. The experimental data for Fig. 6 were taken from Sheindli *et al.* [50] and the agreement is good.

Further checks on this calculation included checking the formation energy of the Dienes defect in 288-atom cells, obtaining 5.14 eV, very close to the value used in Fig. 6. The uniqueness of the Dienes defect proposal was examined by calculating the properties of the spiro-interstitial, which yielded $E_f = 5.85$ eV and $S_f = 5.8 k_B$ at 3500 K. The full temperature dependence of S_f is given in Fig. 7, justifying the use of equation (4) with temperature independent entropy for temperatures above 2000 K. The associated contribution to heat capacity is given as a broken line in Fig. 6 and it does not account for the experimental data.

Discussion

Looking at the heat capacity measurements, if the activation entropy is the same as the formation entropy, and the activation energy is 9 eV, then the rate of formation of Dienes defects is about 1 per second at 2700 K, given an attempt frequency of 10^{13} Hz. This does appear consistent with at least the possibility of achieving an equilibrium concentration for the temperatures at which the divergent heat capacity is reported. The heat capacity results would be dependent on the duration of measurement. In this context it should be noted that not all experimental reports exhibit this ultra-high temperature feature, and sometimes it appears at a higher temperature.

Our calculation gives the Dienes defect concentration is 10^{-7} per atom at 2500 K rising to 10^{-3} at 3600 K and so for this interpretation of heat capacity to hold, it would require that the etching of Dienes defects does not occur in the same way as vacancies, otherwise they would be detected by the technique of ref. 54, which sets an upper limit on their concentration which is not compatible with these high values.

The thermodynamic parameters for the spiro-interstitial does not appear close enough to model the divergent heat capacity and, as with the vacancy, production in the bulk would have to proceed through Frenkel pair formation with an activation of at least 14 eV, so unless there is a strong contribution of graphene edges, it will be ruled out kinetically.

Conclusions

The impact of the discovery of fullerenes is still being felt in the nanoscience of carbons and in revivifying the science of graphite. Here we have reviewed, briefly and selectively according to our purpose, the development of thinking about fullerene isomerization, including catalysis by trace hydrogen and by carbon atoms. The concepts appear to be transferrable from fullerenes, through carbon nanotubes to graphene and graphite, although nanotubes have not been the focus of this work. It is this unifying thread through carbon materials that illustrates the profound nature of the discovery of fullerenes [1] and its ramifications.

In this article we have shown that catalysis concepts offer explanations for the absence of evidence for Dienes or Stone-Wales defects in graphite irradiated by neutrons at reactor temperatures. In addition we have provided new data on the mobilisation of vacancies around these defects and their catalytic effect on defect removal.

The final section challenged the accepted wisdom that the divergent heat capacity of graphite at ultra-high temperature arises from reversible vacancy formation, and gave evidence for the reversible formation of Dienes defects instead, supported by the direct observations of these defects in carbon nanotubes.

Acknowledgements

The authors are grateful to Professor P.R. Briddon and Dr. M.J. Rayson of the University of Newcastle for the provision of the AIMPRO code. MIH thanks Prof. C.P. Ewels for discussions and Professor Sir Harry Kroto F.R.S. for friendship, inspiration and encouragement over the last twenty years.

Funding Statement

MIH, GLH and CDL were funded by British Energy Generation and MIH and CDL are funded by EDF Energy Generation. TT is funded by Innovate UK. The views expressed in this article are those of the authors and do not necessarily represent those of the sponsors.

Competing Interests

We have no competing interests.

Authors' Contributions

MIH drafted the introduction, discussion and conclusion and compiled the results and methodology sections with contributions from GLH who performed the original heat capacity and entropy calculations, CDL who confirmed, improved and added to these calculations, including the spiro-interstitial, and TT who performed the vacancy catalysed destruction of Dienes defect calculations. All authors commented on and approved the subsequent and final revisions.

References

1. H.W. Kroto, J.R. Heath, S.C. O'Brien, R.F. Curl, R.E. Smalley. 1985. C₆₀: Buckminsterfullerene. *Nature* **318**, 162-163. (doi: 10.1038/318162a0)
2. A.J. Stone, D.J. Wales. 1986. Theoretical studies of icosahedral C₆₀ and some related species. *Chem. Phys. Lett.* **128**, 501-503 (doi: 10.1016/0009-2614(86)80661-3)
3. R.B. Woodward, R. Hoffmann. 1969. The Conservation of Orbital Symmetry. *Angew. Chem. Int. Ed.* **8** (11), 781-853. (doi:10.1002/anie.196907811)
4. R. Taylor, J.P. Hare, A.K. Abdul-Sada, H.W. Kroto. 1990. Isolation, separation and characterisation of the fullerenes C₆₀ and C₇₀: the third form of carbon. *J. Chem. Soc., Chem. Commun.* 1423-1425 (doi: 10.1039/C39900001423)
5. P.W. Fowler, D.E. Manolopoulos. 1995. An Atlas of Fullerenes (Clarendon Press: Oxford) ISBN 0-486-45362-6
6. R.L. Murry, D.L. Strout, G.K. Odom, G.E. Scuseria. 1993. Role of sp³ carbon and 7-membered rings in fullerene annealing and fragmentation. *Nature*, **366** 665 - 667 (doi: 10.1038/366665a0)
7. H.F. Bettinger, B.I. Yakobson, G.E. Scuseria. 2002. Scratching the Surface of Buckminsterfullerene: The Barriers for Stone-Wales Transformation through Symmetric and Asymmetric Transition States. *JACS* **125**, 5572-5580 (doi: 10.1021/ja0288744)
8. M.I. Heggie, C.D. Latham, R. Jones and P.R. Briddon. 1995. Local Density Functional Modelling of the Stone-Wales Transformation in Fullerenes. *Recent Advances in the Chemistry And Physics of Fullerenes*: **2**, 1218-1223 eds. K. M. Kadish, R. S. Ruoff, The Electrochemical Society, Pennington.
9. M.I. Heggie, B.R. Eggen, C.P. Ewels, P. Leary, S. Ali, G. Jungnickel, R. Jones, P.R. Briddon. 1995. LDF Calculations of point defects in graphites and fullerenes. *Electrochemical Society Proceedings*, **98-8** 60-67
10. R. Jones, 1989. Ab initio calculations of the structure and properties of large atomic clusters. *Mol. Simulation*, **4**(1-3) 113-120 (doi: 10.1080/08927028908021968)
11. S.K. Estreicher, C.D. Latham, M.I. Heggie, R. Jones, S. Öberg. 1992. Stable and meta-stable states of C₆₀H: buckminsterfullerene monohydride. *Chem. Phys. Lett.* **196**, 311

12. B.R. Eggen, M.I. Heggie, G. Jungnickel, C.D. Latham, R. Jones, P.R. Briddon, 1996. Autocatalysis during fullerene growth. *Science* **272**, 87-89 (doi: 10.1126/science.272.5258.87)
13. C.P. Ewels, M.I. Heggie, P.R. Briddon. Adatoms and nanoengineering of carbon. 2002. *Chemical Physics Letters* **351** 178–182 (doi: 10.1016/S0009-2614(01)01371-9)
14. D. Wales, M.A. Miller, T.R. Walsh. 1998. Archetypal energy landscapes. *Nature* **394**, 758.
15. C.P. Ewels, H.W. Kroto, X. Rocquefelte, M.J. Rayson, P.R. Briddon, M.I. Heggie. 2015. Predicting experimentally stable allotropes: instability of penta-graphene. *Proc. Nat. Acad. Sci (USA)*, **112** (51) 15609-15618 (doi: 10.1073/pnas.1520402112)
16. P.W. Dunk, N.K. Kaiser, C.L. Hendrickson, J.P. Quinn, C.P. Ewels, Y. Nakanishi, Y. Sasaki, H. Shinohara, A.G. Marshall, H.W. Kroto. 2012. Closed network growth of fullerenes. *Nat. Commun.*, **3** 855-855 (doi: 10.1038/ncomms1853)
17. M. Endo, H.W. Kroto. 1992. Formation of carbon nanofibers. *J. Phys. Chem.* **96**, 6941–6944 (doi: 10.1021/j100196a017)
18. M. Kabir, S. Mukherjee, T. Saha-Dasgupta. 2011. Substantial Reduction of Stone-Wales Activation Barrier in Fullerene. *Phys. Rev. B*, **84**, 205404 (doi: 10.1103/PhysRevB.84.205404)
19. I-H. Lee, S. Jun, H. Kim, S.Y. Kim, Y. Lee. 2006. Adatom-assisted structural transformations of fullerenes. *App. Phys. Lett.* **88** 011913 (doi: 10.1063/1.2161175)
20. Calculations of the formation energy of vacancies in graphite crystals, C.A. Coulson, M.D. Poole. 1964. *Carbon*, **2**(3) 275-279 (doi: 10.1016/0008-6223(64)90042-9)
21. A.P.P. Nicholson, D.J. Bacon. 1975. A defect molecule calculation for the vacancy in graphite. *Carbon*, **13**(4) 275-282 (doi: 10.1016/0008-6223(75)90028-7)
22. A. Zunger, R. Englman. 1978. Self-consistent LCAO calculation of the electronic properties of graphite. II. Point vacancy in the two-dimensional crystal. *Phys. Rev. B*, **17** (2) 642-661 (doi: 10.1103/PhysRevB.17.642)
23. A.A. El-Barbary, R.H. Telling, C.P. Ewels, M.I. Heggie, P.R. Briddon. 2003. *Phys. Rev. B*, **68**(14), 1441071-1441077 (doi: 10.1103/PhysRevB.68.144107)
24. E. Kaxiras, K.C. Pandey. 1988. Energetics of defects and diffusion mechanisms in graphite. *Phys. Rev. Lett.* **61**(23) 2693–2696 (doi:10.1103/PhysRevLett.61.2693)
25. G. J. Dienes. 1952. Mechanism for self-diffusion in graphite. *J. Appl. Phys.* **23** (11) 1194–1200 (doi:10.1063/1.1702030)
26. M. Monthioux, J-C. Charlier. 2014. Giving credit where credit is due: The Stone–(Thrower)–Wales designation revisited, Editorial, *Carbon*, **75** 1-4 (doi: 10.1016/j.carbon.2014.03.054.)
27. J.C. Meyer, C. Kisielowski, R. Erni, M.D. Rossell, M.F. Crommie, A. Zettl. 2008. Direct Imaging of Lattice Atoms and Topological Defects in Graphene Membranes. *Nano Lett.*, **8**, 3582–3586 (doi: 10.1021/nl801386m)
28. F. Banhart, J. Kotakoski, A.V. Krasheninnikov. 2011. Structural Defects in Graphene. *ACS Nano* **5**, 26–41 (doi: N. Mounet, N. Marzari. 2005. First-principles determination of the structural, vibrational and thermodynamic properties of diamond, graphite, and derivative *Phys. Rev. B*, **71**(20) 205214 (doi: 10.1103/PhysRevB.71.205214)
29. J. Ma, D. Alfè, A. Michaelides, E. Wang. 2009. Stone-Wales Defects in Graphene and Other Planar sp²-Bonded Materials. *Phys. Rev. B*, **80**, 033407 (doi: 10.1103/PhysRevB.80.033407)
30. C. Wang, Y Ding. 2013. Catalytically healing the Stone–Wales defects in graphene by carbon adatoms. *J. Mater. Chem. A*, **1** 1885-1891 (doi: 10.1039/C2TA00736C)
31. M.R. Nimlos, J. Filley, J.T. McKinnon. 2005. Hydrogen atom mediated Stone-Wales rearrangement of pyracyclene: a model for annealing in fullerene formation. *J Phys Chem A*. **109**, 9896-9903. (doi: 10.1021/jp053441j)
32. A.J.M. Nascimento, R.W. Nunes. 2013. Lubrication of Stone-Wales Transformations in Graphene by Hydrogen and Hydroxyl Functional Groups. *Nanotechnology*, **24**(43), 435707 (doi: 10.1088/0957-4484/24/43/435707)
33. A. I. Podlivaeva, L. A. Openov. 2015. Effect of Hydrogen Adsorption on the Formation and Annealing of Stone-Wales Defects in Graphene. *Physics of the Solid State*, **57** (12) 2562–2569 (doi: 10.1134/S1063783415120276)
34. S.T. Skowron, V.O. Koroteev, M. Baldoni, S. Lopatin, A. Zurutuza, A. Chuvilin, E. Besley. 2016. Reaction kinetics of bond rotations in graphene. *Carbon*, **105** 176-182 (doi: 10.1016/j.carbon.2016.04.020)

35. G. B. Neighbour (Ed.), Management of ageing in graphite reactor cores, Special Publications, The Royal Society of Chemistry, Cambridge, 2007. (doi:10.1039/9781847557742)
36. R.H. Telling, M.I. Heggie. 2007. Radiation Defects in Graphite. *Philos. Mag.* **87**, (31) 4796-4846 (2007) (doi:10.1080/14786430701210023)
37. A.J. McKenna, T. Trevethan, C. D. Latham, P. J. Young, M. I. Heggie. 2016. Threshold displacement energy and damage function in graphite from molecular dynamics. *Carbon* **99** 71-78 (doi:10.1016/j.carbon.2015.11.040)
38. P.O. Lehtinen, A.S. Foster, A. Ayuela, A. Krasheninnikov, K. Nordlund and R.M. Nieminen. 2003. Magnetic properties and diffusion of adatoms on a graphene sheet. *Phys. Rev. Lett.*, **91**, 017202 (doi: 10.1103/PhysRevB.69.073402)
39. P.O. Lehtinen, A.S. Foster, Y. Ma, A.V. Krasheninnikov and R.M. Nieminen. 2004. Irradiation-induced magnetism in graphite: a density functional study. *Phys. Rev. Lett.*, **93**, 187202 (doi: 10.1103/PhysRevLett.93.187202)
40. F. Banhart, J. Kotakoski and A.V. Krasheninnikov. 2010. Structural defects in graphene. *ACS nano*, **5**, 26-41 (doi: 10.1021/nn102598m)
41. R.H. Telling, C.P. Ewels, A.A. El-Barbary, M.I. Heggie. 2003. Wigner defects bridge the graphite gap. *Nat. Mater.*, **2** 333-337 (doi: 10.1038/nmat876)
42. A. Gulans, A.V. Krasheninnikov, M. J. Puska, R.M. Nieminen. 2011. Bound and free self-interstitial defects in graphite and bilayer graphene: A computational study. *Phys. Rev. B* **84**, 024114 (doi:10.1103/PhysRevB.84.024114)
43. H. Zhang, M. Zhao, X. Yang, H. Xia, X. Liu, Y. Xia. 2010. Diffusion and coalescence of vacancies and interstitials in graphite: A first-principles study. *Diamond and Related Materials* **19**(10) 1240-1244 (doi: 10.1016/j.diamond.2010.06.010)
44. P. A. Thrower, R. M. Mayer. 1978. Point defects and self-diffusion in graphite. *Phys. Stat. Sol. A* **47** (1) 11-37 (doi:10.1002/pssa.2210470102)
45. C. D. Latham, M. I. Heggie, M. Alatalo, S. Öberg, P. R. Briddon. 2013. The contribution made by lattice vacancies to the Wigner effect in radiation-damaged graphite. *J. Phys.: Cond. Matt.* **25** (13) 135403 (doi:10.1088/0953-8984/25/13/135403)
46. J.I. Paredes, P. Solís-Fernández, A. Martínez-Alonso, J.M.D. Tascón. 2009. Atomic vacancy engineering of graphitic surfaces: controlling the generation and harnessing the migration of the single vacancy. *J. Phys. Chem. C* **113**(23) 10249019255 (doi: 10.1021/jp901578c)
47. A.S. Fedorov, D.A. Fedorov, Z.I. Popov, Y.E. Ananeva, N.S. Eliseeva, A.A. Kuzubov. 2011. Mobility of vacancies under deformation and their effect on the elastic properties of graphene. *JETP* **112**(5), 820-824 (doi: 10.1134/S1063776111040042)
48. T. Trevethan, C.D. Latham, M. I. Heggie, P.R. Briddon, M.J. Rayson. 2014. Vacancy diffusion and coalescence in graphene directed by defect strain fields. *Nanoscale*, **6**(5) 2978-2986 (doi:10.1039/c3nr06222h)
49. N. Mounet, N. Marzari. 2005. First-principles determination of the structural, vibrational and thermodynamic properties of diamond, graphite, and derivative *Phys. Rev. B*, **71**(20) 205214 (doi: 10.1103/PhysRevB.71.205214)
50. A.E. Sheindli, I.S. Belevich, I.G. Kozhevni. 1973. Enthalpy and specific heat of graphite in temperature range 273-3650 K. *High Temperatures*, **10**(5), 897-900
51. N.S. Rasor, J.D. McClelland. 1960. Thermal properties of graphite, molybdenum and tantalum to their destruction temperature, the physics and chemistry of solids. *J. Phys. Chem. Solids*, **15**, 17-26 (doi:10.1016/0022-3697(60)90095-0)
52. A. Savvatimskiy, S. Onufriev, A. Kondratyev. 2016. Capabilities of pulse current heating to study the properties of graphite at elevated pressures and at high temperatures (up to 5000 K). *Carbon* **98**, 534-536 (doi: 10.1016/j.carbon.2015.11.044)
53. B.T. Kelly, 1981. *The Physics of Graphite* (Applied Science: London) p195.
54. G.R. Hennig. 1964. Determination of lattice vacancies in graphite. *J. Chem. Phys.* **40** (10) 2877-82 (doi: 10.1063/1.1724920)
55. K. Suenaga, H. Wakabayashi, M. Koshino, Y. Sato, K. Urita, S. Iijima. 2007. Imaging active topological defects in carbon nanotubes. *Nature Nano*. **2**, 358- 360 (doi:10.1038/nnano.2007.141)

56. M. Yoon, J. Howe, G. Tibbetts, G. Eres, Z. Zhang. 2007. Polygonization and anomalous graphene interlayer spacing of multi-walled carbon nanofibers. *Phys. Rev. B*, **75** 165402 1-6 (doi:10.1103/PhysRevB.75.165402)
57. P.R. Briddon, R. Jones. 2000. LDA calculations using a basis of Gaussian orbitals. *Phys. Stat. Sol. B* **217**, 131-171 (doi: 10.1002/(SICI)1521-3951(200001))
58. M.J. Rayson, P.R. Briddon. 2008. Rapid iterative method for electronic-structure eigenproblems using localised basis functions. *Comp. Phys. Commun.* **178** (2) 128-134 (doi: 10.1016/j.cpc.2007.08.007)
59. J.P. Goss, M.J. Shaw, P.R. Briddon. 2007. Marker-method calculations for electrical levels using Gaussian-orbital basis sets. Theory of defects in semiconductors. Eds. D.A. Drabold, and S.K. Estreicher, (Springer-Verlag: Berlin Heidelberg) **104** Chapter 3, 69-94 (doi:10.1007/11690320_4)
60. J.P. Perdew, Y.Wang. 1992. Accurate and simple analytic representation of the electron-gas correlation energy. *Physical Review B* **45(23)** 13244 (doi:10.1103/PhysRevB.45.13244)
61. C. Hartwigsen, S. Goedecker, J. Hutter. 1998. Relativistic separable dual-space Gaussian pseudopotentials from H to Rn. *Phys. Rev. B*, **58** 3641-3662 (doi: 10.1103/PhysRevB.58.3641)
62. H.J. Monkhorst, J.D. Pack. 1976. Special points for Brillouin-zone integrations. *Phys. Rev. B*, **13(12)** 5188-5192. (doi: 10.1103/PhysRevB.13.5188)
63. G. Henkelman, B.P. Uberuaga, H. Jonsson. 2000. A Climbing-Image NEB Method for Finding Saddle Points and Minimum Energy Paths. *J. Chem. Phys.* **113** 9901-4 (doi: 10.1063/1.1329672)
64. Thermal properties of harmonic lattice vibrations. Chapter 7 in *Thermophysical Properties of Materials*, G. Grimvall.1999. 112-135, (Elsevier: Amsterdam) (doi 10.1016/B978-044482794-4/50008-5)
65. Equation 4.66 in ref. 50 has a small typographical error which is corrected in our equation 3 and the definition has been altered from specific to molar heat capacity.
66. G.L. Haffenden, M.I. Heggie Using First Principles Calculations to Estimate Thermal Properties of Graphite and its Defects. Brian Kelly Award lecture, Carbon 2009, Biarritz, France

Figures

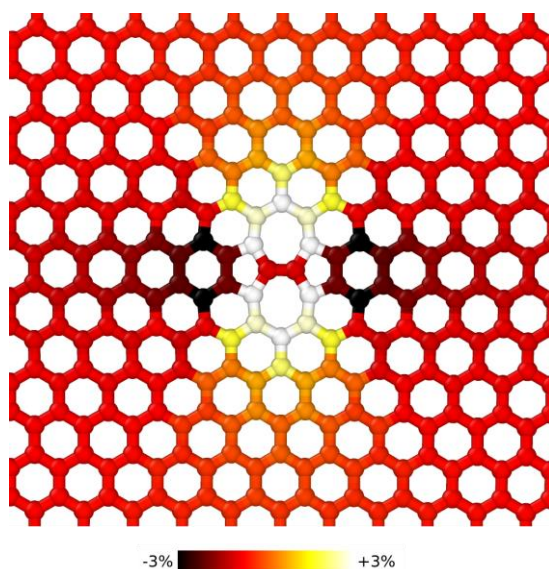


Figure 1 Optimised structure of the Dienes defect in graphene. The atoms are coloured according to the volume (area) of the corresponding Wigner-Seitz cell, which gives a measure of the in-layer strain (Black is compressive and white is tensile)

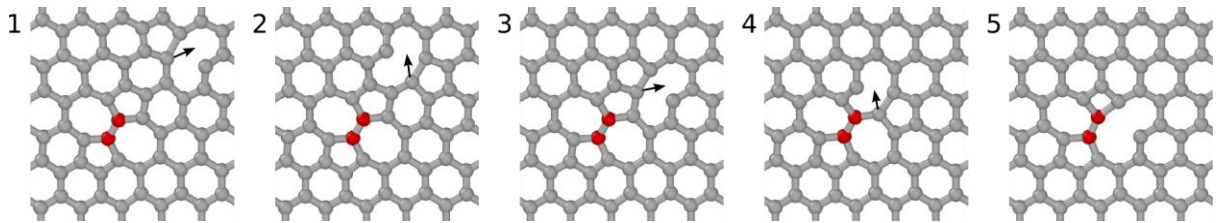


Figure 2 Series of five configurations for the diffusion of a mono-vacancy towards a Dienes defect (the rotated pair of atoms forming the Dienes defect are highlighted in red)

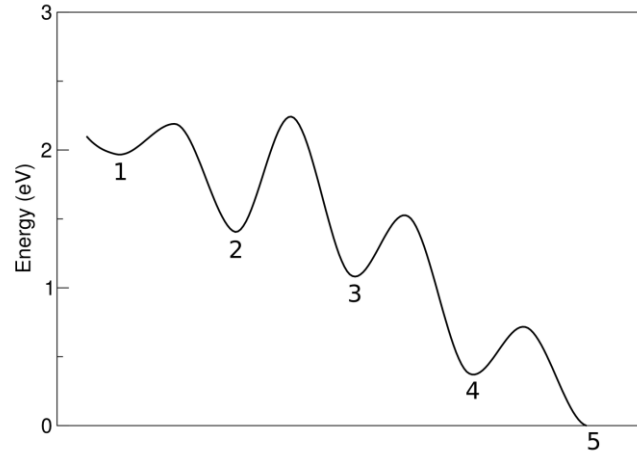


Figure 3 Potential energy surface for the migration of the monovacancy towards the Dienes defect, where the minima are each given a label corresponding to the appropriate configuration of Fig. 2.

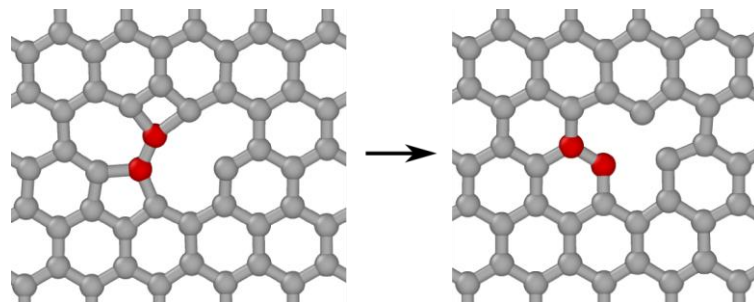


Figure 4 The final bond rotation in configuration 5 removing the Dienes defect leaving the mono-vacancy. The two atoms originally at the core of the Dienes defect are highlighted.

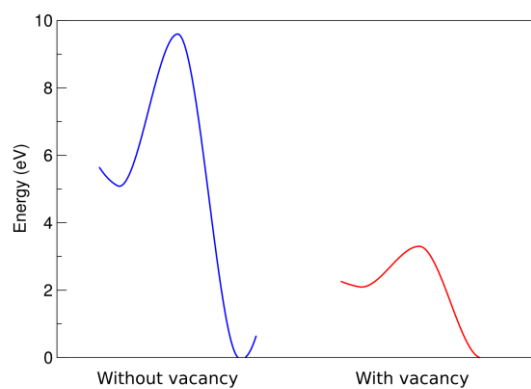


Figure 5 Dienes defect energy profiles: (left) where a mono-vacancy is separated from the defect with no interaction and (right) where the mono-vacancy has diffused toward the defect to form an intimate complex (the structure on the left of Fig. 4).

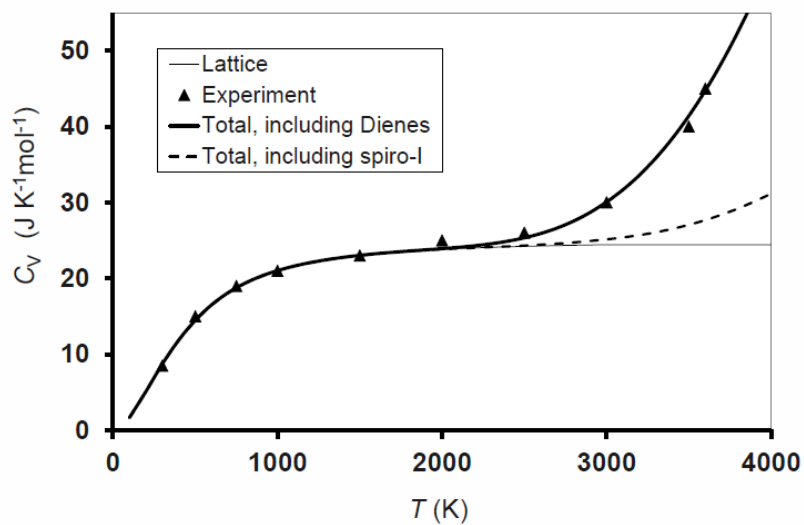


Figure 6 Graphite molar heat capacity with defect contribution from Dienes defects (solid line) and spiro-interstitials (broken line). The thin solid line is the lattice heat capacity of the lattice and the triangular symbols are the experimental data of Sheindli et al. [50].

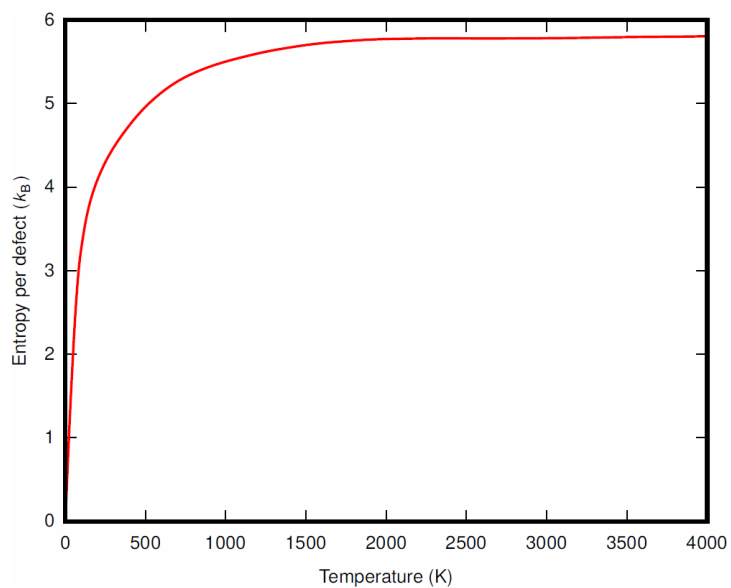


Figure 7 Entropy of the spiro-interstitial